Claudin-2 limits pancreatitis development through regulating tight junction-controlled pancreatic ductal transport.

Sneha Kesaraju[1]*, Yueying Li[1,2]*, Melissa Tracy[1], Kristin Wannemo[1], Joseph Kainov[1], Niyati Rana[1], Mohammed Sidahmed[1], Sanjiv Hyoju[3], Lexi Smith[1], Jonathan Matthews[5], Fatemeh Khalili-Araghi[6], Maunak Rana[4], Scott A. Oakes[1#], Le Shen[3#], Christopher R. Weber[1#]

1. Department of Pathology, The University of Chicago, Chicago, IL, USA
2. Department of Pathology, Wuhan University Zhongnan Hospital, Wuhan, China
3. Department of Surgery, The University of Chicago, Chicago, IL, USA
4. Department of Anesthesia and Critical Care, The University of Chicago, Chicago, IL, USA
5. Pritzker School of Molecular Engineering, The University of Chicago, Chicago, IL, USA
6. Department of Physics, University of Illinois Chicago, IL, USA

*These authors contributed equally

#Corresponding Authors

ABSTRACT

Chronic pancreatitis is a long-term inflammatory disease that results in irreversible scarring and a reduction in pancreatic function. This disease has multifactorial origins, involving both behavioral risks like diet, alcohol, and smoking, as well as genetic predispositions. One gene that has been implicated is *CLDN2*, which encodes claudin-2, a paracellular cation-selective channel localized at tight junctions. However, if and how claudin-2 may modify pancreatitis susceptibility have not been explored. We aimed to clarify the potential role of claudin-2 in the onset and progression of pancreatitis.

We employed multiple methodologies, including examining human pancreatic tissue, using the caerulein-induced experimental pancreatitis model, along with normal pancreatic ductal epithelial cell based organoid transport studies. In both human chronic pancreatitis tissues and in caerulein-induced experimental pancreatitis model, claudin-2 protein is significantly upregulated in pancreatic ductal epithelial cells. Genetically modified mice that lack claudin-2 expression develop more severe experimental pancreatitis, indicating claudin-2 plays a protective role in pancreatitis development. Our organoid based studies further demonstrate claudin-2 is critical for both sodium-dependent water transport and cAMP-dependent fluid secretion in pancreatic ductal epithelium. These findings suggest that intact claudin-2 function is essential for homeostatic and induced fluid transport, which could reduce pancreatitis severity by affecting pancreatic ductal secretion.

In conclusion, our studies suggest claudin-2 upregulation during pancreatitis may play a protective role for disease development and decreased claudin-2 function may increase pancreatitis severity. This points to the possibility of modulating pancreatic ductal claudin-2 function as an approach for pancreatitis therapy.

INTRODUCTION

Chronic pancreatitis is characterized by persistent long-term inflammation and auto-digestion of the pancreas that can lead to permanent scaring of pancreatic tissue (Beyer *et al*., 2020). The most common symptoms include abdominal pain, nausea, vomiting, and oily stools. Chronic pancreatitis can lead to malnutrition due to exocrine pancreatic insufficiency, diabetes due to endocrine dysfunction, and an increased risk of pancreatic ductal adenocarcinoma. In the United States, the annual incidence of chronic pancreatitis is 5 to 8 per 100,000 adults and the prevalence ranges from 42 to 73 per 100,000 adults (Vege & Chari, 2022). Besides the well-recognized lifestyle risk factors, including alcohol and tobacco abuse, genetic factors also contribute to pancreatitis development (e.g., mutations of *PRSS1*, *SPINK1*, *CTRC*, *CASR*, and *CFTR*) (Singh *et al*., 2019). Through genome wide association studies, the *rs12688220* locus with the TT variant has been identified as a risk variant for pancreatitis. Because it its proximity to the *CLDN2* gene, it has been named as the *CLDN2* locus (Deng & Li, 2020; Derikx *et al*., 2015; Giri *et al*., 2016; Masamune *et al*., 2015; Whitcomb *et al*., 2012).

Claudins are tight junction proteins that regulate paracellular permeabilities of small molecules, particularly ions and water. While some claudins form barriers to limit small molecule transport, other claudins can create size and charge selective pores that allow specific molecules to pass through the tight junction, thus controlling paracellular transport (Shen *et al*., 2011). Expression of distinctive combinations of claudin family members is thought to contribute to unique transport properties of different epithelia. It is recognized that claudin-2 forms a cation selective ion channel that controls paracellular Na^+ and Ca^{2+} transport, and it also has been suggested to be a water channel. It is well recognized that in inflammatory diseases, particularly intestinal inflammatory diseases such as inflammatory bowel disease, infectious colitis, and celiac disease have increased claudin-2 expression (Denizot *et al*., 2012; Heller *et al*., 2005; Liu *et al*., 2013; Prasad *et al*., 2005; Schmitz *et al*., 1999; Szakál *et al*., 2010). In healthy pancreas, claudin-2 is primarily expressed in ductal cells, along with weak expression in the acinar cells (Rahner *et al*., 2001). It has been proposed that in chronic pancreatitis patients with CLND2 risk genotype (*rs12688220*, TT is high risk allele), claudin-2 localization is different than patients with the low-risk genotype. Despite these findings, little is known about how the *rs12688220* risk allele is

associated with the increased risk for pancreatitis. For example, despite of the gene locus naming, other genes are located close the *rs12688220* locus, including *MORC4*. Indeed, a number of the genetic studies have also named *rs12688220* locus as the *CLDN2-MORC4* locus (Deng & Li, 2020; Derikx *et al*., 2015; Giri *et al*., 2016; Masamune *et al*., 2015; Whitcomb *et al*., 2012). Thus, it remains unclear if *CLDN2* is a responsible gene within the *rs12688220* locus that contributes to the risk of pancreatitis development. Furthermore, the expression and localization of claudin-2 in patients with or without the risk allele remain to be poorly understood. Claudin-2 expression and distribution has not been compared between healthy individuals with or without the risk allele, and the potential expression and localization change during pancreatitis development in both groups of patients has not been determined. Despite the reported subcellular localization differences of claudin-2 between chronic pancreatitis patients with or without the high-risk allele, this study remains to be preliminary, and if such putative localization differences have any functional consequences has yet to be defined (Deng & Li, 2020; Derikx *et al*., 2015; Giri *et al*., 2016; Masamune *et al*., 2015; Whitcomb *et al*., 2012).

We now demonstrate that claudin-2 expression is upregulated in chronic pancreatitis patients, a phenomenon also observed in the caerulein treatment model of experimental pancreatitis. Studies using *Cldn2* knockout (KO) mice show that they are more susceptible to caerulein injection induced pancreatic alterations, and *Cldn2* KO diminishes stimulated fluid transport across pancreatic ductal epithelium. Taken together, our data show that intact claudin-2 function limits pancreatitis development through regulating paracellular fluid transport in pancreatic ducts.

RESULTS

Claudin-2 expression is upregulated in human chronic pancreatitis.

Previous studies demonstrated that in pancreas, claudin-2 is predominantly expressed in pancreatic ductal epithelial cells, with low expression in pancreatic acinar cells. However, how claudin-2 expression may be altered in chronic pancreatitis remains to be determined. To investigate this, we evaluated claudin-2 expression in pancreatectomy specimens from patients with chronic pancreatitis of various etiologies and non-pancreatitis diseases with normal

pancreatic histology. H&E staining showed acinar cell loss and fibrosis in the chronic pancreatitis samples, which was not present in normal pancreas samples (Fig. 1A). Claudin-2 expression was significantly higher in the ducts of chronic pancreatitis tissues compared to normal pancreas, as determined by immunohistochemical staining (n=13 for pancreatitis samples and n=6 for normal pancreas samples; $p < 0.0001$). (Table 1, Fig. 1B – 1C). Similar results were also obtained when tissues were stained using immunofluorescence microscopy (Fig. 1D). These data suggest claudin-2 may be involved in the pathophysiological processes associated with chronic pancreatitis.

Table 1. Patient characteristics

Patient	Chronic pancreatitis etiology	Comorbidities	Tobacco use	Sex	Age	claudin-2 expression normalized to avg of control
1	Idiopathic	T2DM	No	M	56	1.34
2	Idiopathic	Obesity	Yes	M	79	1.37
3	Alcohol use	T2DM	No	M	53	1.68
4	Idiopathic	none	No	F	67	1.77
5	Alcohol use	T1DM	Yes	M	54	1.45
6	Alcohol use	none	Yes	M	49	1.84
7	Hereditary (CFTR)	T1DM	No	F	52	1.38
8	Idiopathic	none	Yes	M	69	1.44
9	Idiopathic	Addison's Disease	No	F	46	1.75
10	Idiopathic	none	No	F	28	1.57
11	Hereditary (PRSS1)	none	No	M	15	1.34
12	Hereditary (SPINK-1)	T1DM	No	M	42	1.26
13	Hereditary (CFTR)	T1DM	No	M	23	1.50

Claudin-2 expression is increased in caerulein-induced experimental pancreatitis in mice.

We next sought to understand how upregulated claudin-2 expression may impact chronic pancreatitis phenotype by using animal models. We first determined if claudin-2 expression also can be modulated in animal models of disease. Experimental pancreatitis was induced by repeated injection of the cholecystokinin homolog caerulein. Following eight hourly caerulein injections per day for two days, pancreatic samples were collected 1d after the final injection (day 2), representing the early phase of caerulein-induced experimental pancreatitis and 7 d after the final injection (day 8), representing the late phase of the disease (Fig. 1A). H&E staining showed that tissues obtained during early and late phases of disease exhibited histological evidence of tissue damage, including mild expansion of the interstitial space due to edema and inflammation (Fig. 2B). In the late phase of disease, fibrosis was more predominant, particularly in periductal areas (Fig. 2B). Immunohistochemical staining showed claudin-2 expression was

increased in the ductal epithelial cells in both the early (p=0.0145), and late (p=0.0049) phases of disease (Fig. 2C-D). This indicates claudin-2 expression is similarly increased in an animal model of pancreatitis, suggesting this model could be used to investigate how claudin-2 expression change could contribute to pancreatitis development.

Cldn2 KO exacerbates tissue inflammation in the early phase of caerulein-induced experimental pancreatitis.

To determine the contribution of claudin-2 in pancreatitis development, we assessed how claudin-2 expression may impact development of caerulein-induced pancreatitis by using *Cldn2* KO mice. Both control and *Cldn2* KO mice had similar weight change overtime (Supplementary Fig. 1A). In the early phase (1 d after last caerulein injection) of pancreatitis, H&E staining showed that there is more significant tissue reorganization in *Cldn2* KO mice following caerulein treatment (Fig. 3A), and immunohistochemical staining showed that while there was very low claudin-2 staining in pancreas tissues in control and *Cldn2* KO mice without treatment, caerulein only induced significant claudin-2 staining increase in *Cldn2* sufficient control mice (Fig 3B). In this phase, little tissue fibrosis occurred in either control or *Cldn2* KO mice, as indicated by limited blue staining in the trichrome stained tissue (Fig. 3C, E). Immunohistochemical staining of CD45, a pan-leukocyte marker, was performed to assess tissue inflammation. While the percent of total cells staining positive for CD45 in pancreata from both control and *Cldn2* KO mice increased following caerulein treatment, the number increased more in *Cldn2* KO mice (Fig. 3D, F, n=8 and n==8 for control and *Cldn2* KO groups, respectively). This indicates claudin-2 limits tissue inflammation in the early phase of caerulein-induced experimental pancreatitis.

Cldn2 KO exacerbates pancreatic fibrosis in late phase of caerulein-induced experimental pancreatitis.

We next evaluated how the lack of claudin-2 expression affects the late phase (7 d after last cerulean injection) of experimental pancreatitis. At this phase, there was no significant difference in weight between the groups (Supplementary Fig. 1B). In contrast, there was still significant tissue organization differences between control and *Cldn2* KO mice (Fig. 4A). Trichrome

staining showed that although there was still limited fibrosis in control mice, there was significant tissue fibrosis in *Cldn2* KO mice. (n=14 and 17 for control and *Cldn2* KO groups, respectively; p=0.0072) (Fig. 4A-C, Supplementary Fig. 2). CD45 immunohistochemical staining showed the percent of CD45 positive leukocytes in this later phase was lower in both groups of mice, with no statistical significance in both groups, although there was still a small number of *Cldn2* KO mice that had high numbers of tissue leukocytes. Thus, claudin-2 limits tissue fibrosis in the late phase of experimental pancreatitis.

Claudin-2 regulates pancreatic ductal epithelial transport.

Claudin-2 is primarily expressed in pancreatic ductal epithelial cells, and its expression is upregulated in this cell type. Furthermore, claudin-2 can form a paracellular channel that is selective for small cations and can also mediate water transport, based on studies on intestinal and renal epithelium (Muto *et al*., 2010; Tsai *et al*., 2017). Thus, it is possible that claudin-2 can also regulate small cation and water transport in pancreatic ductal epithelium. To test this possibility, we generated pancreatic ductal epithelial organoids from control and *Cldn2* KO mice. Immunofluorescent staining of formalin fixed organoid sections confirmed that claudin-2 is expressed in control organoids, while no claudin-2 expression can be observed in *Cldn2* KO organoids (Fig. 5A).

We hypothesized that if a sodium selective pathway is important for pancreatic ductal epithelial transport, creating an isoosmotic Na^+ gradient across the epithelial layer of a pancreatic organoid would create a driving force for unidirectional Na^+ transport. If Na^+ flows through such a selectively permeable pathway, water must follow to maintain ionic equilibrium (Fig. 5B). To test this, we substituted Na^+ in extraluminal imaging media with isomolar claudin-2 impermeable large organic ion N-methyl-D-glutamine ($NMDG^+$), creating a high intraluminal to extraluminal Na^+ concentration gradient (Fig. 5B). While changing regular imaging media with the same Na^+ containing media had little effect on organoid size, substitution with isoosmotic $NMDG^+$ containing Na^+ free media caused progressive decrease in organoid size (Fig. 5C, D row 2 vs. row 1). In contrast, when such ion substitution was performed on *Cldn2* KO organoids, such size

change was limited (Fig. 5C, D row four vs. row 3). This shows that a Na^+ driven fluid transport pathway exists in pancreatic ductal epithelium, which is claudin-2 dependent.

Claudin-2 participates in secretagogue-induced pancreatic ductal epithelial secretion.

Having identified that claudin-2 can regulate Na^+ dependent transport in pancreatic ductal epithelium, we next sought to assess contributions of claudin-2 to active pancreatic ductal secretion. By using a forskolin induced organoid swelling assay *(Dekkers et al., 2013; Molnár et al*., 2020). In this assay, forskolin activates adenylate cyclase and induces cystic fibrosis transmembrane regulator (CFTR)-mediated cellular secretion of Cl^- into the organoid lumen (Fig. 6A). This generates an electrochemical gradient that drives Na^+ entry into the lumen *(Madácsy et al*., 2018). In control pancreatic ductal epithelial organoids, forskolin induced an increase in organoid size. (Fig. 6B, C). In contrast, forskolin only caused a limited increase in *Cldn2* KO organoid size. These data further show a functional paracellular Na^+ permeable claudin-2 channel is required for pancreatic ductal epithelial secretion.

DISCUSSION

Chronic pancreatitis is a persistent inflammatory disease of the pancreas and originates from a complex interplay of etiologies. These include genetic factors, environmental triggers, autoimmune diseases, and metabolic disorders (Beyer *et al*., 2020). Genetic factors implicated in chronic pancreatitis often mediate changes in the trypsin-dependent pathway, including genes such as *PRSS1*, *SPINK1*, and *CTRC*. Other genes such as *CFTR* and the *CASR* affect the regulation of ion and fluid balance in the pancreatic ducts (Mounzer & Whitcomb, 2013). In addition to these genes, GWAS studies have identified *CLDN2* as a risk gene for acute and chronic pancreatitis (Deng & Li, 2020; Weiss *et al*., 2018; Whitcomb *et al*., 2012). However, if claudin-2 can regulate pancreatitis development remains to be determined.

Here we assessed the role of claudin-2 in pancreatitis development using human tissue, a mouse model, and pancreatic ductal organoids. First, using pancreatic specimens from patients with chronic pancreatitis of various etiologies, we demonstrated that claudin-2 expression is upregulated, particularly in pancreatic ductal cells. Second, we showed that claudin-2 expression is elevated in both the early and late phases of caerulein-induced mouse pancreatitis. Mouse model studies further showed *Cldn2* genetic deletion exacerbates experimental pancreatitis development. Finally duct epithelial function was assessed using organoid models derived from the *Cldn2* KO mice, revealing that claudin-2 is required for efficient fluid handling during pancreatic secretion. These data demonstrate that claudin-2 is a key factor in maintaining ion homeostasis within pancreatic duct and loss of this pathway contributes to pancreatitis development.

For our physiological studies, we used an organoid based system. This is advantageous to previously used 2D model systems, which primarily used tumor derived epithelial cells, as organoid based studies use non-transformed cells that more closely mimic normal epithelial cell function and tissue organization. In addition, this model is more readily implemented with higher throughput than studies using isolated pancreatic ducts. Our present study using such organoids provides previously unrecognized aspects of pancreatic ductal epithelial transport. Experiments substituting extraluminal Na^+ with $NMDG^+$ caused progressive decrease in organoid size, showing a net fluid extrusion from organoid lumen. Because net water movement in our experimental system only occurs in the presence of a local osmotic gradient, our observation suggests Na^+ and $NMDG^+$ movement along their respective concentration gradients across the epithelium is asymmetrical. This shows a size-selective cation permeable pathway exists within the pancreatic ductal epithelium that drives fluid transport. Because this pathway is mostly eliminated in *Cldn2* KO organoids, and claudin-2 mediates size selective- and cation selective-paracellular transport, these data suggest a Na^+ gradient drives fluid transport primarily through a claudin-2 dependent paracellular pathway.

During pancreatic secretion, CFTR mediated Cl^- secretion, and the subsequent $Cl^-/HCO3^-$ exchange through SLC26 family members drives $HCO3^-$ and fluid secretion in the pancreatic ducts (Pallagi *et al*., 2015). It is well recognized that a paracellular shunt pathway is

required for Na^+ to follow anion secretion (Frizzell & Schultz, 1972). However, the molecular entity that creates this paracellular passive Na^+ permeable pathway is unknown. In addition to the result discussed in the above paragraph demonstrating claudin-2 dependent Na^+ permeable pathway exists, our forskolin-induced swelling assay further suggest paracellular Na^+ transport during pancreatic ductal secretion is also mediated by claudin-2.

Although claudin-2 has also been reported to function as a water transporter, and our data show loss of claudin-2 function can limit fluid transport in both organoid models used in this study, it is not clear if observed water transport is directly mediated by claudin-2. It is possible that claudin-2 controlled directional paracellular Na^+ transport only provide an osmotic gradient that drives water transport through other channels, including aquaporins. It is also possible that both passive Na^+ and water transport are directly mediated by claudin-2. Relative contributions of water transport directly through claudin-2 channels and other water transporters remain to be investigated in the future.

Our studies using chronic pancreatitis patient samples and caerulein-induced mouse experimental pancreatitis both showed that claudin-2 protein expression is upregulated in pancreatic ductal epithelium during inflammation. Given results obtained from organoid based studies, such claudin-2 upregulation can facilitate ion and water secretion into the lumen during pancreatitis, and this could be a compensatory pathophysiological change to limit pancreatitis. In the caerulein-induced pancreatitis model, the absence of this upregulation, such as in *Cldn2* KO mice, paracellular Na^+ secretion into the ductal lumen is reduced. This would create a higher luminal Cl^- concentration, limiting further Cl^- secretion and subsequent $Cl^-/HCO3^-$ exchange. At the same time, pH neutral acinar secretion remains undisrupted. This, in combination with reduced claudin-2-dependent pancreatic ductal water secretion, result in reduced secretory volume with neutral pH and increased digestive enzyme concentration. This would lead to elevated spontaneous pancreatic enzyme activation that could cause pancreatic ductal damage. In addition, in severe cases, thickened pancreatic fluid in the case of reduced claudin-2 function may cause ductal obstruction, which also contribute to pancreatitis severity. This leads to increased immune cell infiltration and fibrosis. Mechanistically this is analogous to CFTR

mutation associated pancreatitis, where the driving force for Na^+ and water secretion is reduced by lack of stimulated Cl^- secretion (Angyal *et al*., 2021; Madácsy *et al*., 2018).

The exacerbated caerulein-induced experimental pancreatitis phenotype in *Cldn2* KO mice may be used to explain how *CLDN2* alteration is linked to the *rs12688220* risk allele. The initial genetic study demonstrated that although claudin-2 protein expression is similar in pancreatitis patients with *rs12688220* low (CC or CT) and high (TT) risk alleles, there may be some difference in claudin-2 localization (Whitcomb *et al*., 2012). Although this difference needs to be further confirmed, such change could lead to reduced functional claudin-2 channel at the tight junction, causing increased sensitivity to pancreatitis. It remains to be seen if and how the risk allele cause claudin-2 localization change. Furthermore, contributions of other potential genes near the locus, including *MORC4* and others, remain to be formally tested.

Our data support a role for claudin-2 to limit pancreatitis development, and its function may intersect with other pancreatitis associated risk alleles. It is reported in the small intestine, *Cftr* KO mice have increased claudin-2 expression, which may compensate for the diminished ion transport (De Lisle, 2014). This points to a possibility that claudin-2 upregulation is also higher in patients with pancreatitis risk loci. With ~25% of the pancreatitis patients having the *rs12688220* high risk allele (Whitcomb *et al*., 2012), it is possible a significant number of pancreatitis patients with both *rs12688220* and another risk loci exists, making them have higher risk for and/or more severe pancreatitis.

It is well documented that claudin-2 upregulation is associated with tissue inflammation and fibrosis, two features present in chronic pancreatitis. Many of the inflammatory cytokines, including IL-1β, -6, -9, -13, -22, and tumor necrosis factor (TNF) can upregulate claudin-2 expression (Amoozadeh *et al*., 2015; Mankertz *et al*., 2009; Suzuki *et al*., 2011; Tian *et al*., 2018; Wang *et al*., 2017; Weber *et al*., 2010; Yamamoto *et al*., 2004). Out of these, IL-1β, -6, and TNF are well recognized to be upregulated in pancreatitis (Gómez-Cambronero *et al*., 2002). However, if these cytokines can also impact claudin-2 expression in pancreatic duct epithelium remain to be tested. It worth pointing out that among cytokines that can upregulate claudin-2 expression, IL-22 is unique in that it can limit experimental pancreatitis and associated fibrosis

(Xuan *et al*., 2018). It has also been reported that IL-22 driven claudin-2 expression participates in intestinal crypt secretion, which limits *Citrobacter* induced intestinal inflammation (Tsai *et al*., 2017). These could indicate IL-22 may at least partially exert its protective function through upregulation of claudin-2 expression in pancreatitis. This would also suggest that increasing claudin-2 expression could be a novel therapeutic approach for pancreatitis therapy.

Our studies provide mechanistic insight into the role of claudin-2 in pancreatic ductal epithelial transport and suggest increased claudin-2 expression in pancreatitis is an adaptive response to maintain pancreatic secretion and limit tissue inflammation. Disruption of claudin-2 function led to increased pancreatitis susceptibility. This points to the potential of claudin-2 activating therapy to promote pancreatic secretion and reduce pancreatic inflammation.

METHODS

Human tissue samples

Archival, formalin fixed, paraffin embedded samples of pancreatic tissue were obtained from The Department of Pathology under a protocol approved by The University of Chicago Institutional Review Board. All specimens were from surgical procedures and included six samples of histologically normal pancreas and thirteen samples from patients with non-tumor associated chronic pancreatitis.

Animals and caerulein-induced experimental pancreatitis

Cldn2 knockout (KO) mice (*Cldn2*^{tm1Lex}) on C57BL/6 background were obtained from Alan S. L. Yu (Kansas University Medical Center, Kansas City, KS)(Pei et al., 2016). Mice were maintained by crossing *Cldn2*$^{KO/+}$ female mice with *Cldn2*$^{KO/0}$ male mice at specific pathogen free barrier facility at the University of Chicago, and all procedures were performed with IACUC approval. Due to *Cldn2* being an X-linked gene, *Cldn2*$^{KO/+}$ female mice and *Cldn2*$^{+/0}$ male mice were used as controls, and *Cldn2*$^{KO/KO}$ female mice and *Cldn2*$^{KO/0}$ male mice were used as the *Cldn2* KO group. For caerulein-induced experimental pancreatitis, mice were subjected to 8 hourly intraperitoneal caerulein injection for two consecutive days (from 9 am each day) at a dose of 75

μg/kg body weight (Moore *et al*., 2019). To determine early phase of pancreatitis development, pancreatic samples were harvested 2 d after initiation of caerulein injection (1 d after last injection). For late phase of pancreatitis development, tissue samples were collected 8 d after initiation of caerulein treatment (7 d after last injection) (Moore *et al*., 2019). Tissue samples were immediately fixed after collection with 10% neutral buffered formalin for 24 hours, then transferred in 70% ethanol for tissue embedding.

H&E and trichrome staining

Hematoxylin and eosin (H&E) staining of human samples was performed using a Tissue-Tek Prisma automated slide stainer (Sakura) with attached glass cover slipper. H&E staining of mouse pancreas tissue sections was performed manually. Tissue sections were deparaffinized, rehydrated and stained with hematoxylin. After several washes with water and Scott's bluing reagent, slides were stained with eosin, dehydrated, and mounted. Trichrome staining was performed on formalin fixed paraffin embedded human pancreas tissue and mouse pancreas tissue sections at the Human Tissue Resources Center at The University of Chicago.

Immunohistochemistry and immunofluorescence staining

Immunohistochemical staining for human claudin-2 was performed on formalin fixed paraffin embedded human pancreas tissue sections by using a mouse-anti claudin-2 (1:100, Invitrogen Cat# 32-5600, RRID: AB_2533085). Pancreas sections were deparaffinized, rehydrated and treated with boiling antigen retrieval solution (Vector Laboratories, Burlingame, CA, USA) for 45 minutes. Tissue sections were washed with 3% hydrogen peroxide and blocked with M.O.M IgG blocking solution (Vector Laboratories, Burlingame, CA) for 1 hour. Then tissue sections were washed in 2.5% normal horse serum and incubated in the primary antibody for 30 minutes. Impress polymer reagent (Vector Laboratories, Burlingame, CA) was applied to tissue sections and peroxidase solution (Vector Laboratories, Burlingame, CA) was used for antibody detection. Slides were counterstained with hematoxylin, dehydrated and mounted. For staining of mouse tissues, formalin fixed paraffin embedded tissue sections were stained with rabbit-anti claudin-2 (1:100, Cell Signaling Technology Cat# 28530, RRID: AB_2798961), and rat-anti CD45 (1:100, Invitrogen Cat#14-0451-82, RRID: AB_467251) at the Human Tissue Resources Center at The University of Chicago. Immunofluorescence staining of claudin-2 (1:100, Invitrogen Cat# 32-

5600, RRID: AB_2533085) was performed on formalin fixed paraffin embedded human pancreas tissue and mouse pancreas organoid sections. Sections were washed with 1X TBS-T, quenched with 50 mM NH_4Cl in 1X TBS, blocked, and incubated with the primary antibody overnight. Next, sections were washed with 1X TBS and stained with Alexa Fluor 594 conjugated donkey anti mouse secondary antibody (1:1000, Jackson Immunoresearch, RRID: AB_2340857) and Hoechst 33342 (Thermo Fisher Scientific, Product 953557). ProLong Diamond antifade mountant (Thermo Fisher Scientific, Product P36965) was used for mounting. Immunofluorescence slides were imaged with Keyence BZ-X810 Microscope (Keyence Corporation of America, Itasca, IL).

Quantification of histochemical staining

Trichome, claudin-2, and CD45 stained slides were scanned at 40x magnification using Aperio AT2 slide scanner (Leica Biosystems) and accessed using Aperio eSlide Manager which links to Aperio Imagescope (Leica, v. 12.4.5) software (Leica) for analysis. Slides were annotated manually using Imagescope to select multiple regions of interest for every sample analyzed, which were averaged to provide a single value from each slide for statistical analysis. Trichrome blue staining was quantified using the positive pixel count algorithm v. 8.1 tuned to blue color (Hue center 0.66, Hue width 0.35; Color saturation threshold 0.04, weak intensity 175-220, medium intensity 100-175, strong intensity 0-100). Staining was normalized to total pixels within annotated pancreatic parenchyma. Claudin-2 staining was quantified using the positive pixel count algorithm v. 8.1 tuned to brown color (Hue center 0.1, Hue width 0.5; Color saturation threshold 0.04; weak intensity 175-220, medium intensity 100-175, strong intensity 0-100) and normalized to total pixels within the annotated ducts. CD45 positive cells were quantified using automatic cell membrane detection algorithm v. 9.1, with an intensity threshold range of 0 to 220. Lymphoid aggregates and lymph nodes were excluded from analysis. CD45 positive cells were normalized to total cells within the annotation regions.

Generation and maintenance of organoids

Pancreatic ductal epithelial organoid lines were generated from 6 w old littermate control and *Cldn2* KO mice using published methods, with slight modifications (Huch et al., 2013). Mice were euthanized and pancreas was removed using sterile technique. Pancreas was minced using

surgical scissors and digested with 62.5 µg/mL Collagenase from *Clostridium histolyticum* (Sigma, C9407) and 62.5 µg/mL Dispase II (Gibco, 17105-041), 10 µM Y-27632 (Cayman Chemicals, 10005583) and 100 µg/mL Primocin (InvivoGen, ant-pm-1) in Advanced DMEM/F12 medium (Gibco, 12634010), incubating at 37□ in a shaking incubator for 20 minutes, followed by digestion with TrypLE Express (Gibco, 12605010) and DNase I 0.1mg/mL (Invitrogen, 18047019) for 10 minutes. After trituration, digested samples were filtered through a 100 µm cell strainer. Cells were resuspended in Cultrex UltiMatrix reduced growth factor basement membrane extract (Bio-techne, BME001-05) and plated into prewarmed 24 well plates, and incubated in complete pancreatic organoid growth media (Advanced DMEM/F-12 containing 15 mM HEPES pH7.4 [Gibco 15630130], 50U/mL penicillin-streptomycin [Gibco, 15070063], 100 µg/mL Primocin, 1x serum free B-27 supplement [Gibco, 17504044], 5 mM nicotinamide [MilliporeSigma, N0636], 1.25 mM N-acetylcysteine, [MilliporeSigma, A0737], 10 mM Y-27632, 50 ng/ml EGF (Peprotech AF-100-15), 100 ng/ml FGF-10 [Peprotech, 100-26], 2% Noggin-Fc fusion protein conditioned medium [ImmunoPrecise Antibodies, N002] 2% Rspo3-Fc fusion protein conditioned medium [ImmunoPrecise Antibodies, R001], 5 µM A83-01 [Tocris, 2939], 10 nM [Leu15]-Gastrin I [MilliporeSigma, G9145], 3 µM prostaglandin E_2 [MilliporeSigma, P0409]). Media was replaced every 2 to 3 d. Pancreatic ductal epithelial organoids were passaged by TrypLE express digestion and split at a 1:3 dilution about every 3-5 days.

Time-lapse live imaging of organoids and image quantification

For time-lapse live organoid imaging, control and *Cldn2* KO pancreatic ductal epithelial organoids were digested by TrypLE express then filtered through 40 µm cell strainer. Near single cell suspension was split at 1:100 and embedded in Cultrex UltiMatrix reduced growth factor basement membrane extract in 48 well plates. Organoids were grown in differentiation media (complete pancreatic organoid growth media without A83-01, [Leu15]-Gastrin I, and prostaglandin E_2) for 4-5 d until experimentation, with media change every 2-3 d.

To assess morphological changes of organoids following switching from Na^+ containing media to Na^+ free $NMDG^+$ containing media, organoids grown in differentiation media were first washed once with Hanks' balanced salt solution (HBSS), and incubated with HBSS for 30 min. For

organoids with each genotype, half of the wells were then switched to regular Na^+ containing HBSS (mock treatment), and half of the wells were switched to iso-osmotic HBSS with Na^+ completely substituted with $NMDG^+$. Organoids were imaged every 10 m after initial switching to HBSS by using a BZ-X810 Microscope (Keyence) with a 4 x Plan Fluorite objective (0.13NA PhL, Keyence) for 120 m at ambient temperature.

For the forskolin induced swelling assay, organoids were washed and incubated with regular HBSS for 30 min. For each genotype, half of the wells were then switched to regular HBSS (mock treatment), and half of the wells were switched to HBSS containing 10μm forskolin (Apexbio, B1421). Organoids were imaged every 10 m after initial switching to HBSS by using a BZ-X810 Microscope (Keyence) with a 4 x Plan Fluorite objective for 180 m at ambient temperature.

For organoid size quantification, acquired images were opened in ImageJ and assembled to time-lapse stacks. Files were then analyzed by the in-house developed OrganoID package (Matthews et al., 2022), Area of each organoid was measured and outputted as Excel (Microsoft, Redwood, WA) documents. Organoid areas at different time points were then normalized to their respective starting value for subsequent statistical analyses.

Data analysis and statistics

Statistical analyses and data visualization was done by using Prism 8.0 (GraphPad, San Diego, CA, USA) and data is reported as mean ± SEM. Two-tailed Student's t test was used to compare the mean of two groups, one-way ANOVA with Bonferroni *post hoc* analysis was used for multiple comparisons and repeated measures two-way ANOVA analyses was used to compare multiple groups over multiple time points. Statistical significance is designated as $*p<0.05$, $**p<0.01$, and $***p<0.001$.

ACKNOWLEDGEMENTS

Organoids were developed by The University of Chicago Organoid and Primary Culture Research Core. Histology and digital pathology services were provided by The University of Chicago Human Tissue Research Center Core. Alan Yu at Kidney Institute, University of Kansas Medical Center kindly provided *Cldn2* KO mice. Schematic presentations were generated by using Biorender software. Savas Tay (Pritzker School of Molecular Engineering, The University of Chicago, Chicago, IL, USA) provided analytical tools and conceptual insights.

COMPETING INTERESTS

The authors declare no competing financial interests.

AUTHOR CONTRIBUTIONS

S.A.O, L.Sh., and C.R.W. conceived, developed, and supervised the study. S.K., Y.L., M.T., K.W., J.K., N. R., L.Sm., L.Sh., and C.R.W. performed experiments, S.K., Y.L., M.S., S.H., L. Sh., and C.R.W. performed data analysis, M.R. collected clinical data. J.M. and S.T. developed and improved analytical tools, F.K-H. provided analytical tools and conceptual insights. S.K. Y.L., L.Sh., and C.R.W. drafted and revised the manuscript. All authors reviewed and approved the manuscript.

TABLES:

Table 1: Human chronic pancreatitis health history and claudin-2 quantification.

FIGURE LEGENDS

Figure 1. Claudin-2 protein expression is upregulated in human chronic pancreatitis. A. Representative images of H&E-stained human pancreatic tissue sections. (Scale bar 200 µm) **B.** Claudin-2 immunohistochemical staining of human pancreatic tissue sections. (Top scale bar 200 µm, bottom scale bar 100 µm) C. Quantification of pancreatic ductal epithelial claudin-2 staining. Blue circles: normal pancreas tissue (n=6), red triangles: human chronic pancreatitis tissue (n=13) ($p < 0.0001$). Unpaired Student's *t* test, ***$p<0.001$. **D.** Representative immunofluorescence staining of claudin-2 in human pancreatic tissue sections. (Scale bar 50 µm)

Figure 2. Claudin-2 protein expression is increased in caerulein-induced experimental pancreatitis. A. Timeline of caerulein-induced experimental pancreatitis. Following 8 hourly caerulein injections daily for two days, pancreas samples were harvested during early phase (1 d recovery) and late phase (7 d recovery) of the disease. **B.** Representative images of H&E-stained mouse pancreatic tissue sections. (Scale bar 100 µm) **C.** Claudin-2 staining of mouse pancreatic tissue sections. (Scale bar 100 µm) **D.** Quantification of claudin-2 staining as percent positivity (positive pixels/total pixels in pancreatic ductal epithelium) in pancreatic ducts. Blue circles: untreated mouse pancreas tissue (n=4), red squares: 1 d recovery following caerulein injection (n=4), red triangles: 7 d recovery following caerulein injection (n=8). Two-tailed one-way ANOVA with Bonferroni *post hoc* analysis was used for statistical analysis. *$p<0.05$ and **$p<0.01$. Untreated versus 1d recovery mice: $p=0.015$, untreated versus 7 d recovery: $p=0.0049$.

Figure 3. *Cldn2* KO mice have increased tissue leukocytes in early phase of experimental pancreatitis. Pancreatic tissues were harvested 1 d following caerulein injection. **A.** Representative H&E-stained mouse pancreatic tissue sections. (Top panels: scale bar 1 mm, bottom panels: scale bar 200 µm) **B.** Claudin-2 staining of mouse pancreas tissue sections. (Scale

bar 50 µm) **C.** Trichrome staining of mouse pancreatic tissue sections. (Scale bar 100 µm) **D.** CD45 staining of leukocytes in mouse pancreatic tissue sections. (Scale bar 200 µm) **E.** Quantification of percent collagen/fibrosis staining (blue) area over total tissue area, visualized by trichrome staining. Blue circles: control mice (n=4), red squares: *Cldn2* KO mice (n=4), blue triangles: caerulein treated control mice (n=4), red upside down triangles: caerulein treated *Cldn2* KO mice (n=4) (all comparisons not significant p>0.05). **F.** Quantification of CD45 positive cells. Blue circles: control mice (n=4), red squares: *Cldn2* KO mice (n=4), blue triangles: caerulein treated control mice (n=4), red upside down triangles: caerulein treated *Cldn2* KO mice (n=4) (control untreated vs. control caerulein p=0.0012, *Cldn2* KO untreated vs. *Cldn2* KO caerulein p=0.000009; control caerulein vs. *Cldn2* KO caerulein p=0.017). Two-tailed one-way ANOVA with Bonferroni *post hoc* analysis was used for statistical analysis. **p<0.01, and ***p<0.001.

Figure 4. *Cldn2* KO mice have increased tissue fibrosis during the late phase of experimental pancreatitis. A. Representative H&E-stained mouse pancreatic tissue sections. (Top panels: scale bar 2 mm, bottom panels: scale bar 100 µm) **B.** Trichrome staining of mouse pancreatic tissue sections. (Scale bar 100 µm) **C.** Quantification of percent collagen/fibrosis staining (blue) area over total tissue area, visualized by trichrome staining. Green triangles: caerulein injected control mice (n=14), red triangles: caerulein injected *Cldn2* KO mice (n=17) (p=0.0072)**. D.** CD45 staining of leukocytes in mouse pancreatic tissue sections. (Scale bar 100 µm) **E**. Quantification of CD45+ positive cells. Green triangles: caerulein injected control mice (n=14), red triangles: caerulein injected *Cldn2* KO mice (n=17) (p=0.0942). Two-tailed unpaired Student's *t* test was used for statistical analysis**.** **p<0.01.

Figure 5. Claudin-2 mediates Na^+-gradient-driven water transport in pancreatic ductal epithelium. A. Representative H&E and claudin-2 staining of control and *Cldn2* KO pancreatic ductal epithelial organoid sections. (Scale bars 50 µm) **B.** Schematic presentation of possible mechanism of Na^+ gradient-driven organoid shrinkage. Top panels: no unidirectional water transport when luminal and extraluminal solution both contain Na^+. Bottom panels: when extraluminal Na^+ is substituted with $NMDG^+$, a monovalent cation driving force exists for water to move out of organoid lumen. **C.** Representative time lapse images of organoid within the same

field over time for each treatment condition. Dashed red circles indicate initial organoid outline. Substitution of Na^+ in extraluminal imaging media (HBSS) with isomolar Na^+ (first and third rows) or $NMDG^+$ (second and forth rows) occurred at t=0. (Scale bars 50 µm) **D.** Quantification of normalized organoid area. Green circles and line: control organoids mock changed to Na^+ containing HBSS (n=5), orange squares and line: *Cldn2* KO organoids mock changed to Na^+ containing HBSS (n=9), red triangles and line: control organoids changed to $NMDG^+$ containing HBSS (n=5), upside down blue triangles and line: *Cldn2* KO organoids changed to $NMDG^+$ containing HBSS (n=10) ($p<0.0001$ among different groups). Repeated measures 2-way ANOVA test. ***$p<0.001$.

Figure 6. Claudin-2 mediates forskolin-induced mouse pancreatic ductal organoid swelling. A. Schematic presentation of possible mechanism of forskolin induced organoid swelling. Left panels: no unidirectional water transport occurs at resting state. Right panels: forskolin treatment activate CFTR to induce Cl^- secretion. This leads to SLC26 mediated Cl^-/HCO_3^- exchange, resulting in HCO_3^- secretion. This drives paracellular Na^+ secretion. This creates an osmotic gradient for water secretion. **B.** Representative time lapse images of control and *Cldn2* KO mouse organoids with and without forskolin (FSK) treatment. Red circles indicate initial organoid outline. (Scale bar 50 µm) **C.** Quantification of normalized organoid area. Green squares and line: control organoids without FSK treatment (n=11), blue circles and line: *Cldn2* KO organoids without FSK treatment (n=24), upside down orange triangles and line: control organoids with 10 µM FSK treatment (n=12), red triangles and line: *Cldn2* KO organoids with 10 µM FSK treatment (n=9) ($p<0.0001$). Repeated measures 2-way ANOVA test with. ***$p<0.001$.

Supplementary Figure 1. Weight change in mice with caerulein induced experimental pancreatitis. A. Body weight change up to 2 d after initiation of caerulein treatment. Green squares and line: caerulein treated control mice (n=4), red squares and line: caerulein treated *Cldn2* KO mice (n=4) ($p=0.72$). **B.** Body weight change up to 8 d after initiation of caerulein treatment. Green triangles and line: control mice (n=14), red triangles: *Cldn2* KO mice (n=20) ($p=0.74$). Repeated measures two-way ANOVA was used for statistical analysis.

Supplementary Figure 2. Trichrome stain in 7-day recovery mouse model of pancreatitis. A. Trichrome staining of mouse pancreatic tissue sections. (Scale bar 2 mm). Blue staining highlights collagen. The green and red annotations reflect intrapancreatic lymph nodes which were excluded from the trichrome staining analysis. **B**. Heat map of trichrome collagen staining as generated by Aperio Imagescope positive pixel count algorithm. Blue indicates no fibrosis, and yellow, orange, and red indicate increasing degrees of fibrosis. Percent positivity was determined by dividing all positive pixels by total non-white pixels.

REFERENCES

Amoozadeh, Y., Dan, Q., Xiao, J., Waheed, F., & Szászi, K. (2015). Tumor necrosis factor-α induces a biphasic change in claudin-2 expression in tubular epithelial cells: role in barrier functions. *Am J Physiol Cell Physiol*, *309*(1), C38-50. https://doi.org/10.1152/ajpcell.00388.2014

Angyal, D., Bijvelds, M. J. C., Bruno, M. J., Peppelenbosch, M. P., & de Jonge, H. R. (2021). Bicarbonate Transport in Cystic Fibrosis and Pancreatitis. *Cells*, *11*(1). https://doi.org/10.3390/cells11010054

Beyer, G., Habtezion, A., Werner, J., Lerch, M. M., & Mayerle, J. (2020). Chronic pancreatitis. *Lancet*, *396*(10249), 499-512. https://doi.org/10.1016/s0140-6736(20)31318-0

De Lisle, R. C. (2014). Disrupted tight junctions in the small intestine of cystic fibrosis mice. *Cell Tissue Res*, *355*(1), 131-142. https://doi.org/10.1007/s00441-013-1734-3

Dekkers, J. F., Wiegerinck, C. L., de Jonge, H. R., Bronsveld, I., Janssens, H. M., de Winter-de Groot, K. M., . . . Beekman, J. M. (2013). A functional CFTR assay using primary cystic fibrosis intestinal organoids. *Nat Med*, *19*(7), 939-945. https://doi.org/10.1038/nm.3201

Deng, Y., & Li, Z. (2020). Effects of PRSS1-PRSS2 rs10273639, CLDN2 rs7057398 and MORC4 rs12688220 polymorphisms on individual susceptibility to pancreatitis: A meta-analysis. *Genomics*, *112*(1), 848-852. https://doi.org/10.1016/j.ygeno.2019.05.025

Denizot, J., Sivignon, A., Barreau, F., Darcha, C., Chan, H. F., Stanners, C. P., . . . Barnich, N. (2012). Adherent-invasive Escherichia coli induce claudin-2 expression and barrier defect in CEABAC10 mice and Crohn's disease patients. *Inflamm Bowel Dis*, *18*(2), 294-304. https://doi.org/10.1002/ibd.21787

Derikx, M. H., Kovacs, P., Scholz, M., Masson, E., Chen, J. M., Ruffert, C., . . . Rosendahl, J. (2015). Polymorphisms at PRSS1-PRSS2 and CLDN2-MORC4 loci associate with alcoholic and non-alcoholic chronic pancreatitis in a European replication study. *Gut*, *64*(9), 1426-1433. https://doi.org/10.1136/gutjnl-2014-307453

Frizzell, R. A., & Schultz, S. G. (1972). Ionic conductances of extracellular shunt pathway in rabbit ileum. Influence of shunt on transmural sodium transport and electrical potential differences. *J Gen Physiol*, *59*(3), 318-346. https://doi.org/10.1085/jgp.59.3.318

Giri, A. K., Midha, S., Banerjee, P., Agrawal, A., Mehdi, S. J., Dhingra, R., . . . Bharadwaj, D. (2016). Common Variants in CLDN2 and MORC4 Genes Confer Disease Susceptibility in Patients with Chronic Pancreatitis. *PLoS One*, *11*(1), e0147345. https://doi.org/10.1371/journal.pone.0147345

Gómez-Cambronero, L. G., Sabater, L., Pereda, J., Cassinello, N., Camps, B., Viña, J., & Sastre, J. (2002). Role of cytokines and oxidative stress in the pathophysiology of acute pancreatitis: therapeutical implications. *Curr Drug Targets Inflamm Allergy*, *1*(4), 393-403. https://doi.org/10.2174/1568010023344544

Heller, F., Florian, P., Bojarski, C., Richter, J., Christ, M., Hillenbrand, B., . . . Schulzke, J. D. (2005). Interleukin-13 is the key effector Th2 cytokine in ulcerative colitis that affects epithelial tight junctions, apoptosis, and cell restitution. *Gastroenterology*, *129*(2), 550-564. https://doi.org/10.1016/j.gastro.2005.05.002

Huch, M., Bonfanti, P., Boj, S. F., Sato, T., Loomans, C. J., van de Wetering, M., . . . Clevers, H. (2013). Unlimited in vitro expansion of adult bi-potent pancreas progenitors through the Lgr5/R-spondin axis. *Embo j*, *32*(20), 2708-2721. https://doi.org/10.1038/emboj.2013.204

Liu, X., Yang, G., Geng, X. R., Cao, Y., Li, N., Ma, L., . . . Liu, Z. (2013). Microbial products induce claudin-2 to compromise gut epithelial barrier function. *PLoS One*, *8*(8), e68547. https://doi.org/10.1371/journal.pone.0068547

Madácsy, T., Pallagi, P., & Maleth, J. (2018). Cystic Fibrosis of the Pancreas: The Role of CFTR Channel in the Regulation of Intracellular Ca(2+) Signaling and Mitochondrial Function in the Exocrine Pancreas. *Front Physiol*, *9*, 1585. https://doi.org/10.3389/fphys.2018.01585

Mankertz, J., Amasheh, M., Krug, S. M., Fromm, A., Amasheh, S., Hillenbrand, B., . . . Schulzke, J. D. (2009). TNFalpha up-regulates claudin-2 expression in epithelial HT-29/B6 cells via phosphatidylinositol-3-kinase signaling. *Cell Tissue Res*, *336*(1), 67-77. https://doi.org/10.1007/s00441-009-0751-8

Masamune, A., Nakano, E., Hamada, S., Kakuta, Y., Kume, K., & Shimosegawa, T. (2015). Common variants at PRSS1-PRSS2 and CLDN2-MORC4 loci associate with chronic pancreatitis in Japan. In *Gut* (Vol. 64, pp. 1345-1346). https://doi.org/10.1136/gutjnl-2015-309802

Matthews, J. M., Schuster, B., Kashaf, S. S., Liu, P., Ben-Yishay, R., Ishay-Ronen, D., . . . Tay, S. (2022). OrganoID: A versatile deep learning platform for tracking and analysis of single-organoid dynamics. *PLoS Comput Biol*, *18*(11), e1010584. https://doi.org/10.1371/journal.pcbi.1010584

Molnár, R., Madácsy, T., Varga, Á., Németh, M., Katona, X., Görög, M., . . . Maléth, J. (2020). Mouse pancreatic ductal organoid culture as a relevant model to study exocrine pancreatic ion secretion. *Lab Invest*, *100*(1), 84-97. https://doi.org/10.1038/s41374-019-0300-3

Moore, P. C., Cortez, J. T., Chamberlain, C. E., Alba, D., Berger, A. C., Quandt, Z., . . . Oakes, S. A. (2019). Elastase 3B mutation links to familial pancreatitis with diabetes and pancreatic adenocarcinoma. *J Clin Invest*, *129*(11), 4676-4681. https://doi.org/10.1172/jci129961

Mounzer, R., & Whitcomb, D. C. (2013). Genetics of acute and chronic pancreatitis. *Curr Opin Gastroenterol*, *29*(5), 544-551. https://doi.org/10.1097/MOG.0b013e3283639383

Muto, S., Hata, M., Taniguchi, J., Tsuruoka, S., Moriwaki, K., Saitou, M., . . . Furuse, M. (2010). Claudin-2-deficient mice are defective in the leaky and cation-selective paracellular permeability properties of renal proximal tubules. *Proc Natl Acad Sci U S A*, *107*(17), 8011-8016. https://doi.org/10.1073/pnas.0912901107

Pallagi, P., Hegyi, P., & Rakonczay, Z., Jr. (2015). The Physiology and Pathophysiology of Pancreatic Ductal Secretion: The Background for Clinicians. *Pancreas*, *44*(8), 1211-1233. https://doi.org/10.1097/mpa.0000000000000421

Pei, L., Solis, G., Nguyen, M. T., Kamat, N., Magenheimer, L., Zhuo, M., . . . Yu, A. S. (2016). Paracellular epithelial sodium transport maximizes energy efficiency in the kidney. *J Clin Invest*, *126*(7), 2509-2518. https://doi.org/10.1172/jci83942

Prasad, S., Mingrino, R., Kaukinen, K., Hayes, K. L., Powell, R. M., MacDonald, T. T., & Collins, J. E. (2005). Inflammatory processes have differential effects on claudins 2, 3 and 4 in colonic epithelial cells. *Lab Invest*, *85*(9), 1139-1162. https://doi.org/10.1038/labinvest.3700316

Rahner, C., Mitic, L. L., & Anderson, J. M. (2001). Heterogeneity in expression and subcellular localization of claudins 2, 3, 4, and 5 in the rat liver, pancreas, and gut. *Gastroenterology*, *120*(2), 411-422. https://doi.org/10.1053/gast.2001.21736

Schmitz, H., Barmeyer, C., Fromm, M., Runkel, N., Foss, H. D., Bentzel, C. J., . . . Schulzke, J. D. (1999). Altered tight junction structure contributes to the impaired epithelial barrier function in ulcerative colitis. *Gastroenterology*, *116*(2), 301-309. https://doi.org/10.1016/s0016-5085(99)70126-5

Shen, L., Weber, C. R., Raleigh, D. R., Yu, D., & Turner, J. R. (2011). Tight junction pore and leak pathways: a dynamic duo. *Annu Rev Physiol*, *73*, 283-309. https://doi.org/10.1146/annurev-physiol-012110-142150

Singh, V. K., Yadav, D., & Garg, P. K. (2019). Diagnosis and Management of Chronic Pancreatitis: A Review. *Jama*, *322*(24), 2422-2434. https://doi.org/10.1001/jama.2019.19411

Suzuki, T., Yoshinaga, N., & Tanabe, S. (2011). Interleukin-6 (IL-6) regulates claudin-2 expression and tight junction permeability in intestinal epithelium. *J Biol Chem*, *286*(36), 31263-31271. https://doi.org/10.1074/jbc.M111.238147

Szakál, D. N., Gyorffy, H., Arató, A., Cseh, A., Molnár, K., Papp, M., . . . Veres, G. (2010). Mucosal expression of claudins 2, 3 and 4 in proximal and distal part of duodenum in children with coeliac disease. *Virchows Arch*, *456*(3), 245-250. https://doi.org/10.1007/s00428-009-0879-7

Tian, L., Li, Y., Zhang, J., Chang, R., Li, J., & Huo, L. (2018). IL-9 promotes the pathogenesis of ulcerative colitis through STAT3/SOCS3 signaling. *Biosci Rep*, *38*(6). https://doi.org/10.1042/bsr20181521

Tsai, P. Y., Zhang, B., He, W. Q., Zha, J. M., Odenwald, M. A., Singh, G., . . . Turner, J. R. (2017). IL-22 Upregulates Epithelial Claudin-2 to Drive Diarrhea and Enteric Pathogen Clearance. *Cell Host Microbe*, *21*(6), 671-681.e674. https://doi.org/10.1016/j.chom.2017.05.009

Vege, S. S., & Chari, S. T. (2022). Chronic Pancreatitis. *N Engl J Med*, *386*(9), 869-878. https://doi.org/10.1056/NEJMcp1809396

Wang, Y., Mumm, J. B., Herbst, R., & Kolbeck, R. (2017). IL-22 Increases Permeability of Intestinal Epithelial Tight Junctions by Enhancing Claudin-2 Expression. *J Immunol*, *199*(9), 3316-3325. https://doi.org/10.4049/jimmunol.1700152

Weber, C. R., Raleigh, D. R., Su, L., Shen, L., Sullivan, E. A., Wang, Y., & Turner, J. R. (2010). Epithelial myosin light chain kinase activation induces mucosal interleukin-13 expression

to alter tight junction ion selectivity. *J Biol Chem*, *285*(16), 12037-12046. https://doi.org/10.1074/jbc.M109.064808

Weiss, F. U., Hesselbarth, N., Párniczky, A., Mosztbacher, D., Lämmerhirt, F., Ruffert, C., . . . Rosendahl, J. (2018). Common variants in the CLDN2-MORC4 and PRSS1-PRSS2 loci confer susceptibility to acute pancreatitis. *Pancreatology*, *18*(5), 477-481. https://doi.org/10.1016/j.pan.2018.05.486

Whitcomb, D. C., LaRusch, J., Krasinskas, A. M., Klei, L., Smith, J. P., Brand, R. E., . . . Devlin, B. (2012). Common genetic variants in the CLDN2 and PRSS1-PRSS2 loci alter risk for alcohol-related and sporadic pancreatitis. *Nat Genet*, *44*(12), 1349-1354. https://doi.org/10.1038/ng.2466

Xuan, X., Tian, Z., Zhang, M., Zhou, J., Gao, W., Zhang, Y., . . . Fan, W. (2018). Diverse effects of interleukin-22 on pancreatic diseases. *Pancreatology*, *18*(3), 231-237. https://doi.org/10.1016/j.pan.2018.02.014

Yamamoto, T., Kojima, T., Murata, M., Takano, K., Go, M., Chiba, H., & Sawada, N. (2004). IL-1beta regulates expression of Cx32, occludin, and claudin-2 of rat hepatocytes via distinct signal transduction pathways. *Exp Cell Res*, *299*(2), 427-441. https://doi.org/10.1016/j.yexcr.2004.06.011

Figure 1

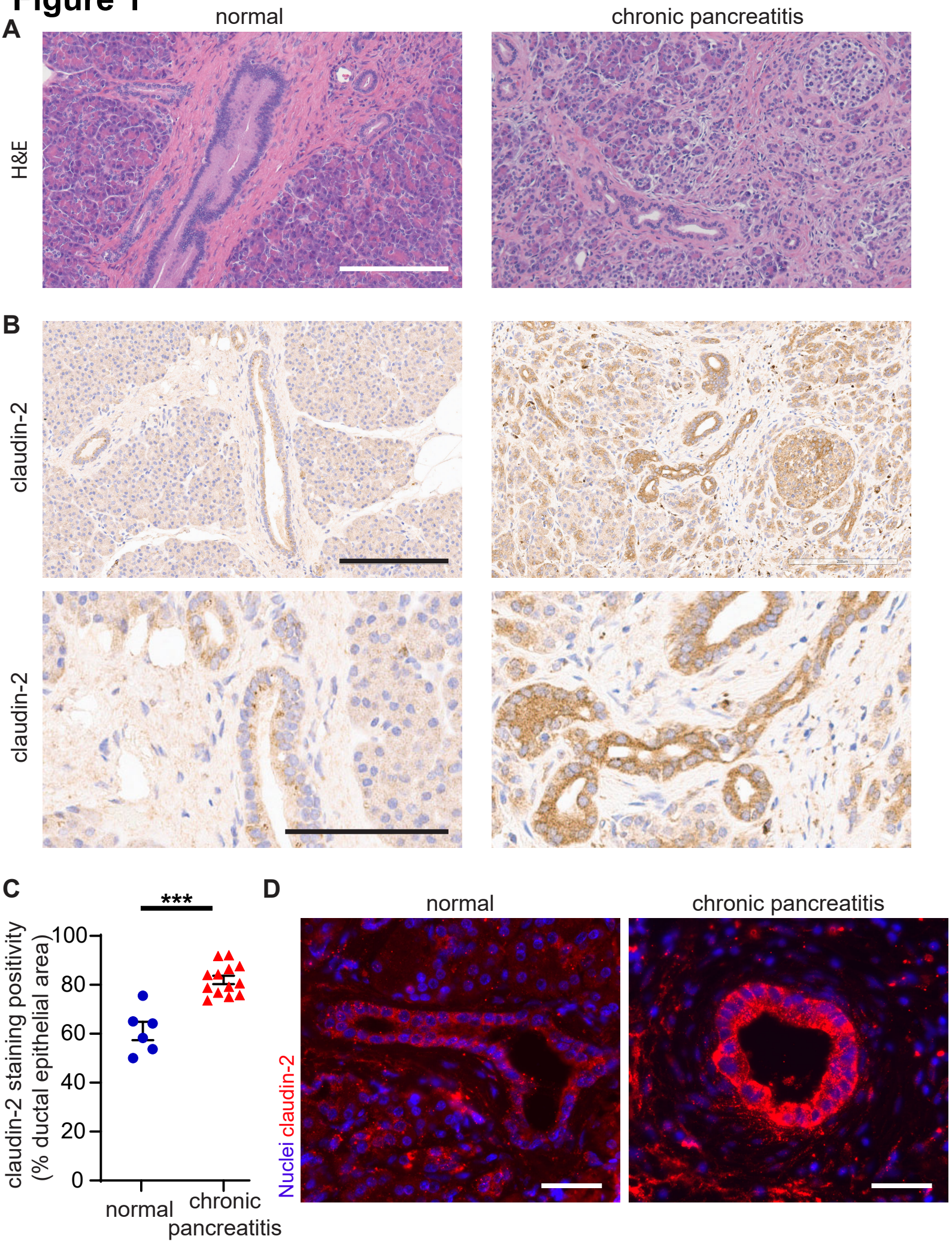
A
normal
chronic pancreatitis
H&E
B
claudin-2
claudin-2
C
***
claudin-2 staining positivity
(% ductal epithelial area)
100
80
60
40
20
0
normal
chronic
pancreatitis
D
normal
chronic pancreatitis
Nuclei claudin-2

Figure 2

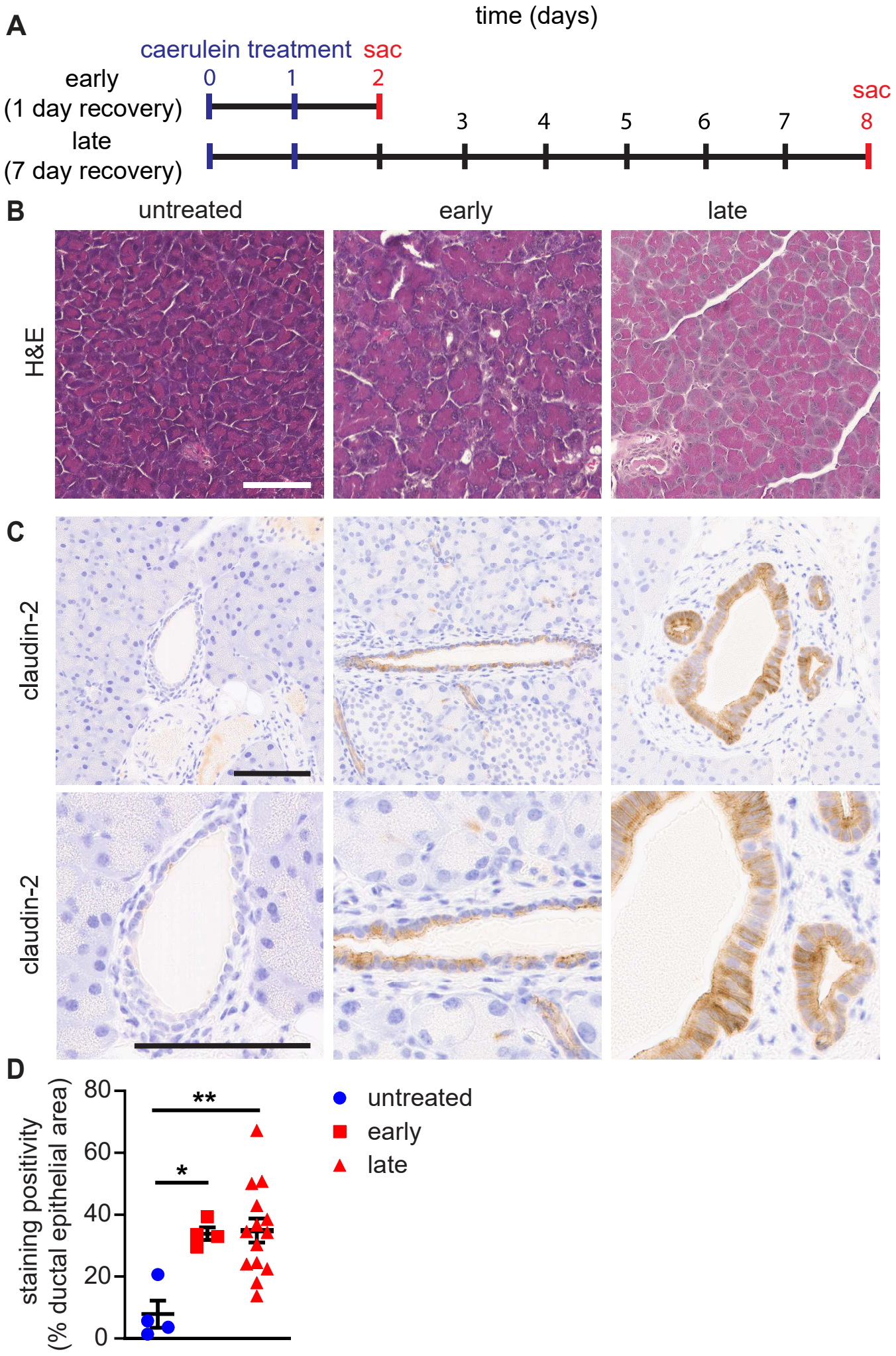
A
time (days)
caerulein treatment
sac
early
(1 day recovery)
late
(7 day recovery)
0
1
2
3
4
5
6
7
8
sac
B
untreated
early
late
H&E
C
claudin-2
claudin-2
D
staining positivity
(% ductal epithelial area)
80
60
40
20
0
**
*
untreated
early
late

Figure 3

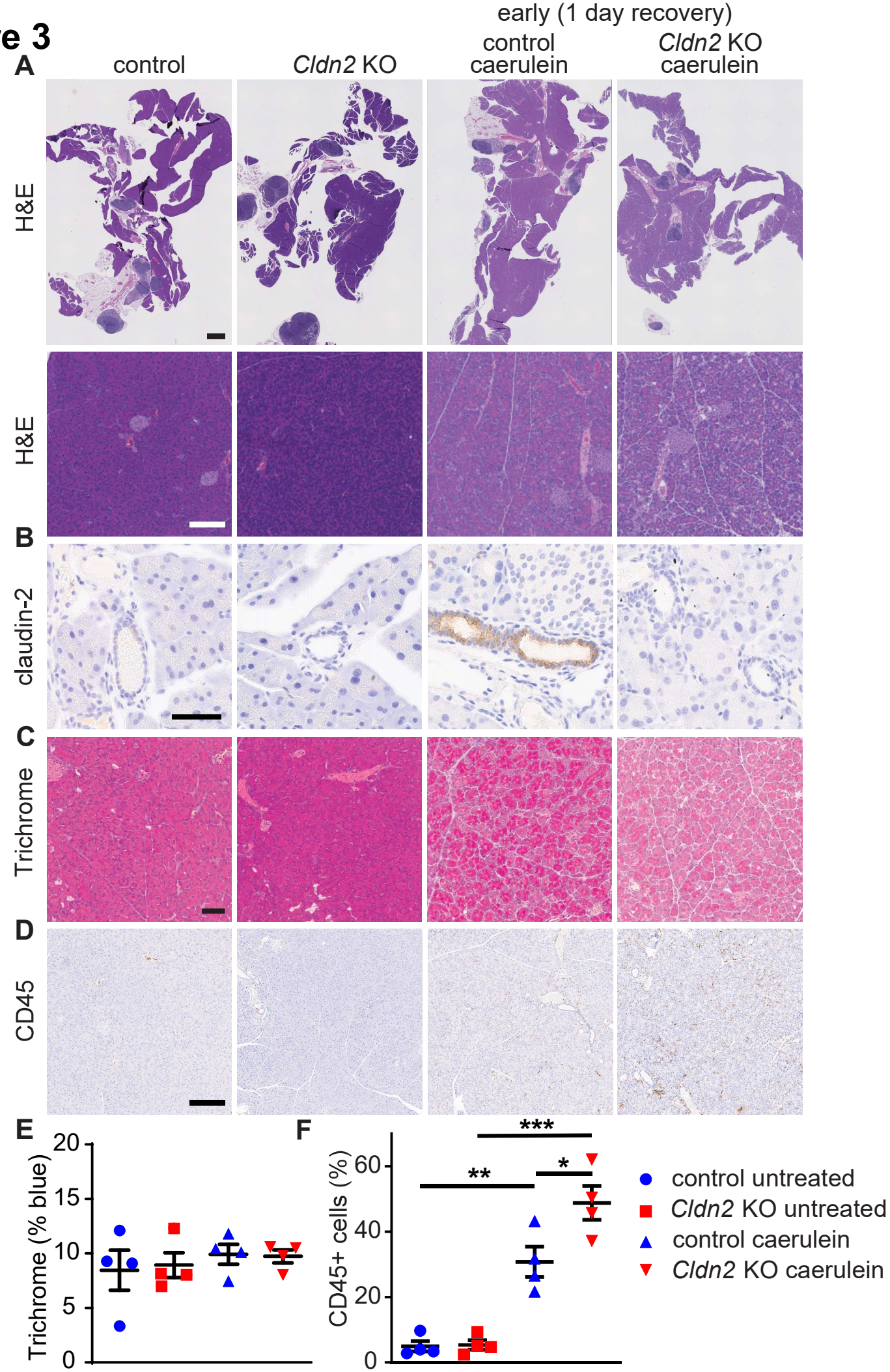
early (1 day recovery)
control
Cldn2 KO
control caerulein
Cldn2 KO caerulein
A
H&E
H&E
B
claudin-2
C
Trichrome
D
CD45
E
Trichrome (% blue)
20
15
10
5
0
F
CD45+ cells (%)
60
40
20
0
***
**
*
control untreated
Cldn2 KO untreated
control caerulein
Cldn2 KO caerulein

Figure 4

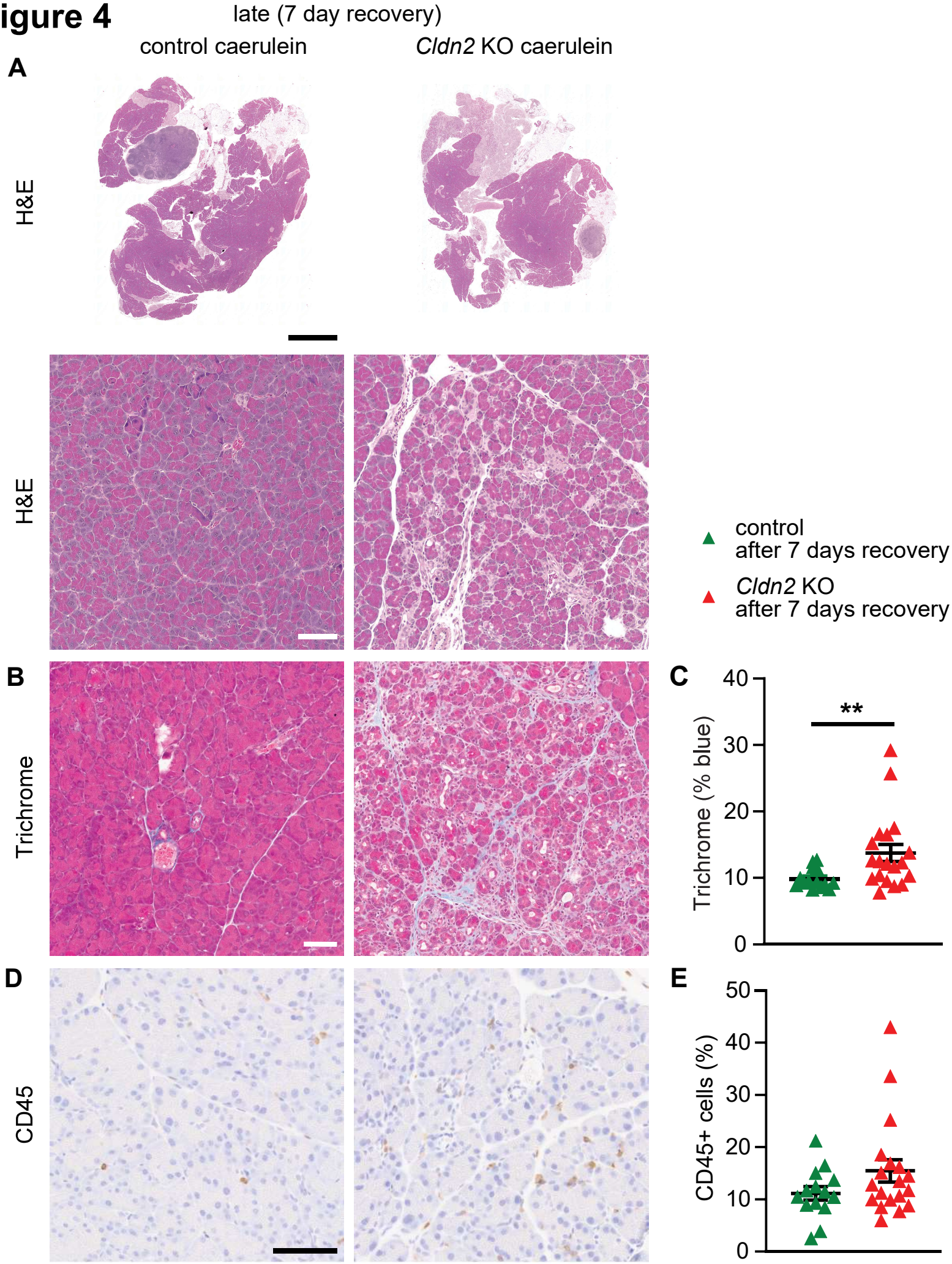
late (7 day recovery)
control caerulein
Cldn2 KO caerulein
A
H&E
H&E
B
Trichrome
D
CD45
control
after 7 days recovery
Cldn2 KO
after 7 days recovery
C
Trichrome (% blue)
40
30
20
10
0
**
E
CD45+ cells (%)
50
40
30
20
10
0

Figure 5

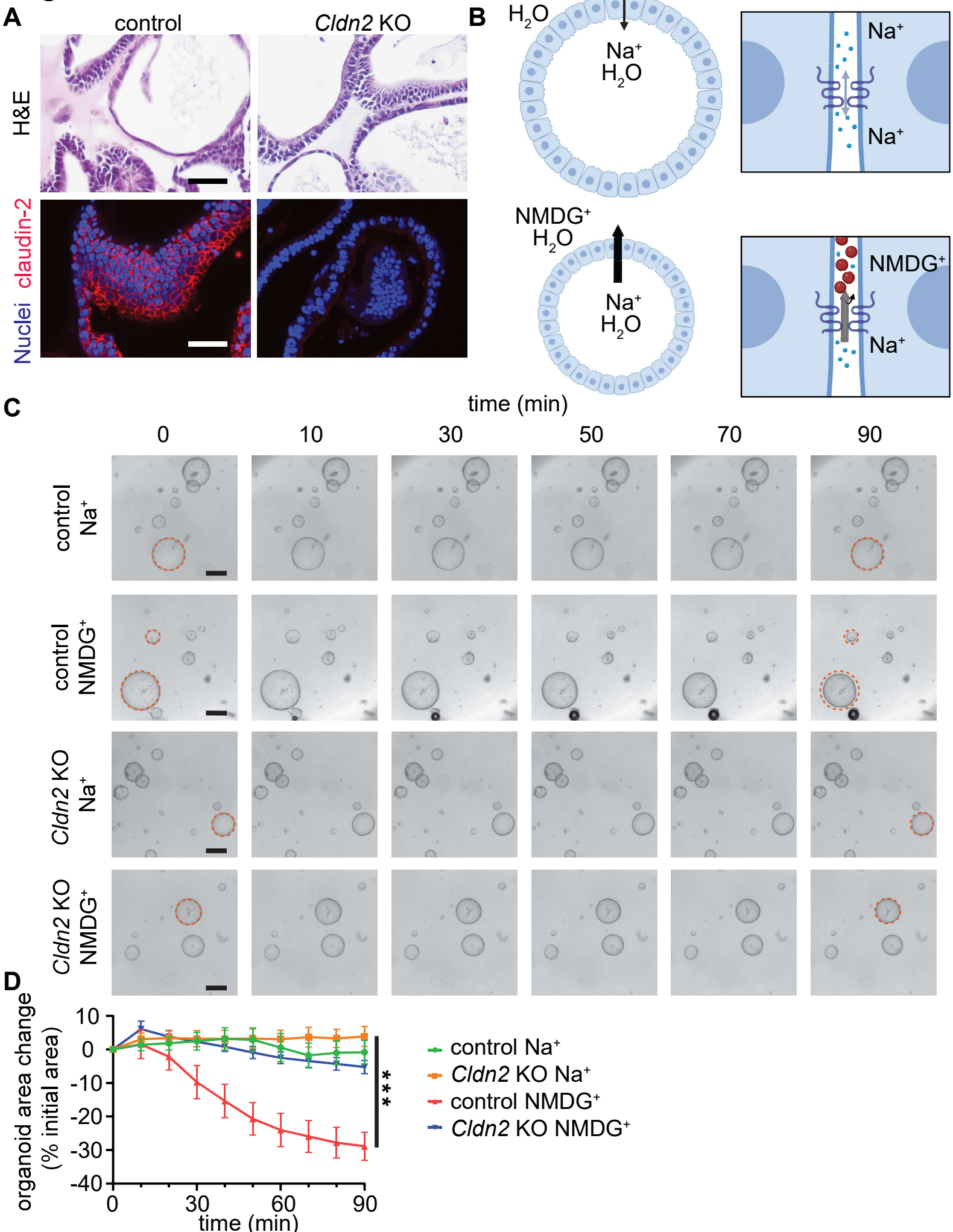
A
control
Cldn2 KO
H&E
Nuclei claudin-2
B
Na+
H2O
Na+
H2O
Na+
Na+
NMDG+
H2O
Na+
H2O
NMDG+
Na+
C
time (min)
0
10
30
50
70
90
control Na+
control NMDG+
Cldn2 KO Na+
Cldn2 KO NMDG+
D
organoid area change (% initial area)
10
0
-10
-20
-30
-40
0
30
60
90
time (min)
***
control Na+
Cldn2 KO Na+
control NMDG+
Cldn2 KO NMDG+

Figure 6

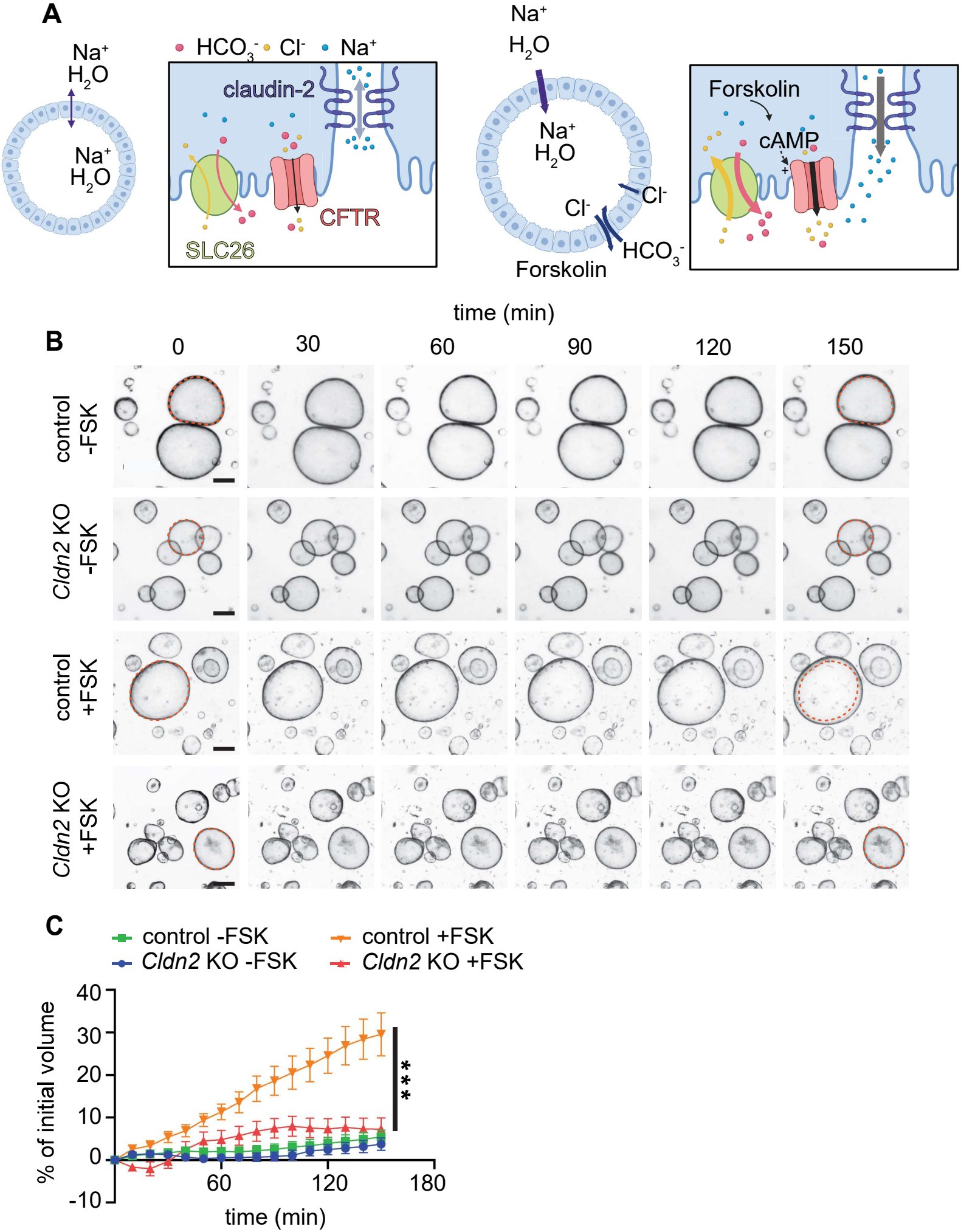
A
Na+
H2O
Na+
H2O
HCO3-
Cl-
Na+
claudin-2
CFTR
SLC26
Na+
H2O
Na+
H2O
Cl-
Cl-
HCO3-
Forskolin
Forskolin
cAMP
B
time (min)
0
30
60
90
120
150
control -FSK
Cldn2 KO -FSK
control +FSK
Cldn2 KO +FSK
C
control -FSK
Cldn2 KO -FSK
control +FSK
Cldn2 KO +FSK
% of initial volume
40
30
20
10
0
-10
60
120
180
time (min)
***

Supplementary Figure 1

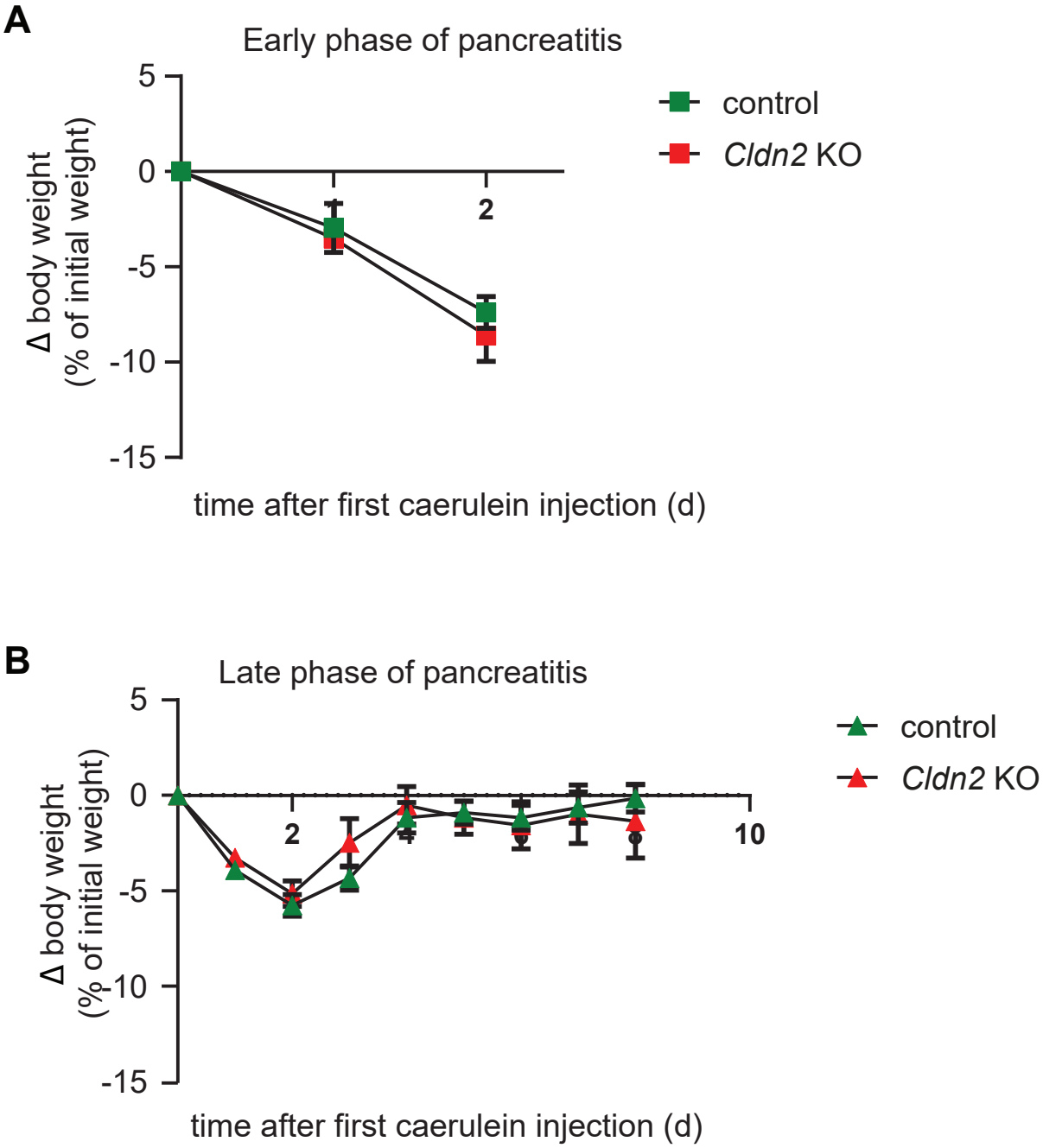
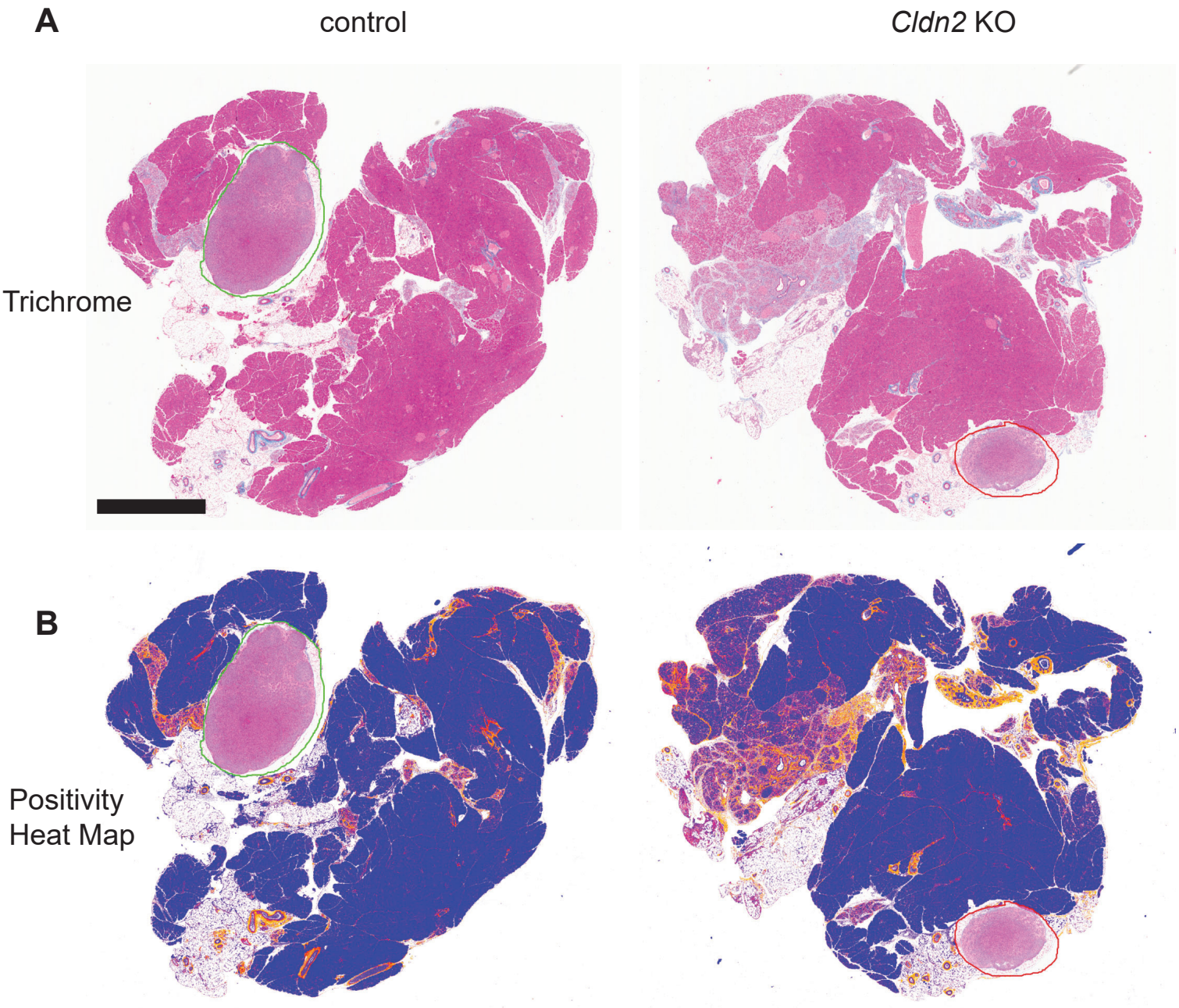
Supplementary Figure 2